Abstract

1 Introduction

1.1 Geological and tectonic summary

- Large scale overview/summary of regions under study

- Justification for selecting these regions?

1.2 Previous geophysical studies

- Lithoprobe and attendent papers

- Teleseismic studies

2 Data and methods

Our analysis of bulk Canadian continental crust is based on estimates of crustal properties that can be accessed via seismic techniques, namely seismic wave velocities (or velocity ratio) and crustal thickness. This study draws on three sources for these crustal properties. The first and primary source is teleseismic receiver function (hereafter RF) analysis. The remaining two datasets are Crust 2.0, a widely published statistical average of similar regions with a global two degree resolution, and a compilation of pre-processed active source data (Mooney, 2012). Both Crust 2.0 and the active source compilation are used to qualify and compare with the primary dataset.

2.1 Teleseismic Data Set

The primary data utilized in this study are computed from teleseismic P wave seismograms originating from more than 700 earthquake sources. These earthquakes occurred between 2000 and 2012 and were recorded on subsets of 343 broadband seismic stations distributed across Canada. Seismic stations are selected from all available regional and national networks including

CNSN, POLARIS, FedNor and Chasme. Seismograms are included for analysis if they fall within a 30 to 100° epicentral distance window. Quality control is performed by admitting only those seismograms with sufficiently high signal to noise ratios to permit visual observation of the dominant P wave energy and with sufficiently impulsive first arrivals to allow arrival onsets to be accurately measured. After selection and filtering more than 80,000 events are available for further processing.

The first stage of processing requires the transformation of teleseismic data into receiver functions. In general terms, this transformation involves deconvolving an approximation of the earthquake source from horizontal recordings of ground motion [Langston, 1979]. The resulting waveforms contain discrete pulses corresponding to S waves scattered from subsurface discontinuities including the base of the crust, or Moho. Confident identification of these peaks is required to estimate crustal parameters, and improved results can be obtained by transforming the displacement seismogram into their P and S contributions based on a 1-D model of propagation. This procedure is accomplished by first rotating the N and E coordinates into radial and transverse directions and then performing a wave field decomposition using the radial and vertical channels [Kennet, 1991]. The direct P arrival of the signal on the resulting P wave component is used as an approximation to the source function as P component impulse response for teleseismic P approximates a delta function. This windowed source estimate is deconvolved from the S wave component computed from the wave field decomposition.

We employ an L_2, multichannel, frequency domain approach to perform the deconvolution that has the advantage of computational efficiency and does not require *a priori* assumptions concerning the noise levels in the data. More specifically, we employ a simultaneous deconvolution of N seismograms sharing a similar slowness to compute a single impulse response or receiver function $r(t)$.

$$r(t) = \mathcal{F}^{-1}\left[G(\omega)\right] = \mathcal{F}^{-1}\left[\frac{\sum_n^N S_n(\omega)P_n^*(\omega)}{\sum_n^N P_n(\omega)P_n^*(\omega) + \delta}\right], \tag{1}$$

where F^{-1} is the inverse Fourier transform, S_n represents the nth S wave seismogram, P_n is the corresponding windowed P wave seismogram, $*$ denotes complex conjugation and δ is the regularization parameter controlling the trade off between model smoothness and data misfit. The parameter δ which is chosen programatically by minimizing the general cross validation function
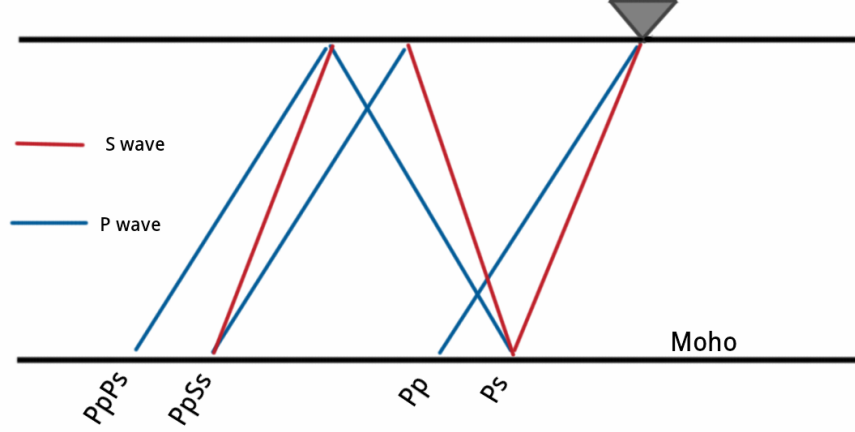
Figure 1: Schematic diagram illustrating geometry of phases for the velocity contrast representing the Moho

$GCV(\delta)$ is given by

$$GCV(\delta) = \frac{\sum_n^N \sum_m^M \left(S_n(\omega_m) - P_n(\omega_m)G(\omega_m)\right)^2}{\left(NM - \sum_m^M X(\omega_m)\right)^2}, \tag{2}$$

where

$$X(\omega_m) = \frac{\sum_n^N P_n(\omega_m)P_n^*(\omega_m)}{\sum_n^N P_n(\omega_m)P_n^*(\omega_m) + \delta}, \tag{3}$$

and ω is the frequency bin in the discrete Fourier transform. All resulting receiver functions, $r(t)$, are filtered between 0.04Hz and 3.0Hz.

2.2   Vp/Vs method

A well tested and widely published method for extracting the ratio of P velocity V_P to S velocity V_S, herafter referred to as R, and crustal thickness (or depth to Moho) H, is outlined by Zhu and Kanamori [2000], hereafter ZK. This method exploits the dependence of these parameters to the differential

3

arrival times between the S wave reflected phases Ps, $PpPs$, $PsPs$, $PpSs$ and $PsSs$ and the direct P wave arrival Pp (Fig 1). Note that $PsPs$ and $PpSs$ are kinematic analogues, such that the energy for these two phases arrive simultaneously for a 1-D model. For a range of slowness values, p, the differential arrival times, $t(p)$, trace moveout curves for each phase arrival given by

$$t_{Ps}(p_n) = \frac{H}{V_P} \left[\sqrt{R^2 - V_P^2 p_n^2} - \sqrt{1 - V_P^2 p_n^2} \right] \tag{4}$$

$$t_{Pps}(p_n) = \frac{H}{V_P} \left[\sqrt{R^2 - V_P^2 p_n^2} + \sqrt{1 - V_P^2 p_n^2} \right] \tag{5}$$

$$t_{Pss}(p_n) = \frac{2H}{V_P} \sqrt{R^2 - V_P^2 p_n^2} \tag{6}$$

where p_n is the slowness for the nth receiver function. Since strong reflected phases occur at sharp velocity contrasts, the Moho, the boundary targeted by ZK, tends to be well represented on most RF's.

The travel time equations, as employed by ZK, assume a value for crustal P wave velocity, V_P, that in practice will trade-off to some degree with crustal thickness H. In our implementation of the ZK approach, each station is assigned a V_P value corresponding to the Crust 2.0 value for the corrisponding $2°$ containing cell. In the specific cases where data are being compared to previously published results for quality control, V_P values are chosen to match the values in the published study.

RFs are stacked along trial moveout curves for a range of candidate models of R and H to generate a fitness function $s(H, R)$. Within the stacking procedure, each phase is assigned a weight to account for the expected relative amplitudes of the phases for typical velocity contrasts, with the direct conversion Ps usually characterized by the highest quality signal followed by $PpPs$ and $PpSs$. We chose weights of $w1 = 0.5$, $w2 = 0.3$, $w3 = -0.2$ for the Ps, $PpPs$ and $PpSs$ phases, respectively. A negative weight for the combined $PpSs$ and $PsPs$ phases is required as the polarity of the signal is reversed. Semblance weighting [Eaton, 2006] is employed to reduce the effect of spurious large amplitude noise in the data. The semblance function assigns a weight between zero (incoherent noise) and one (coherent signal). The stacking function is therefore defined as

$$s(H, R) = \sum_{m=1}^{3} S_m \sum_{n=1}^{N} w_m r_n(t_m) \tag{7}$$

where

$$S_m(H, R) = \frac{\left[\sum_{n=1}^{N} r_n(t_m)\right]^2}{\sum_{n=1}^{N} r_n^2(t_m)} \tag{8}$$

is the semblance weight for the mth phase, time t_m is calculated from the corresponding travel time function for a given H, R pair as a function of slowness p_n and N is the total number of receiver functions. Multiplying by the semblance weighting sharpens the stacked image, $s(H, R)$, and results in better resolution when discriminating between different models. The function $s(H, R)$ can be thought of as a transformation that maps times of the Ps, $PpPs$ and $PpSs+PsPs$ phases into R and H space as positive bands, via Eq. 7. Constructive interference where these bands intersect produce a maximum in the stacking function. The model, R and H, that produces this maximum provides the best estimate for the bulk crustal parameters for a given seismic station.

A limitation of the ZK approach is the requirement of an initial V_P estimate. In principal we may compute the stacking function Eq. 7, as a function of all three seismic parameters, $s(H, R, V_P)$. Taking advantage of modern multi-core systems with reasonable quantities of data (fifty to a few hundred RFs) and a moderate search space (n^3 parameter candidates where $n \approx 150$) the computational time makes this method easily scalable to hundreds of stations. This "fullgrid" approach is analyzed to determine the viability of recovering V_P.

The trade-off between V_P and H (and other parameter combinations) and error resulting from data quality are quantified for both the full parameter search and ZK methods by bootstrap resampling [Efron and Tibshirani, 1986]. An estimate for the error is calculated in a bootstrap resampling approach by taking the standard deviation of 1024 parameter estimates each produced with randomly selected RFs, with replacement.

2.3 Additional data

We supplement receiver function estimates of crustal properties with data from controlled source experiments collected and compiled from GSC (Geo-

logical Survey of Canada) references by Walter Mooney (personal communication, 2012). The active source data provide V_P and a few V_S estimates for hundreds of locations across Canada, many along transects that cross major geological boundaries, faults and discontinuities. Some of these data are located within reasonable (<100 km) proximity to seismic stations used in this study and can be used to compare with the V_P and V_S estimates resulting from the RF full gridsearch.

The Crust 2.0 model [Bassin, 2000] employs many of these same active source data to provide regular, complete coverage across all of Canada. The model includes estimates of V_P and V_S information with depth at 2° resolution in latitude and longitude. In addition to employing local active source data, Crust 2.0 is also constrained by statistically aggregated data from geographically distant but geologically similar regions. It therefore affords a somewhat independent dataset suited for comparison with the crustal estimates calculated in this study.

3   Results

3.1   Comparisons

Three published studies have provided parameter estimates for R and H for subsets of the seismic stations considered here. The most recent study [Thompson et. al., 2010] focused on the northern Canadian Shield and employs both the linear stacking approach used by ZK as well as a phase weighted method. A 2007 study of the Superior Province [Darbyshire et. al, 2007] and a study of the Grenville Orogen [Eaton et. al., 2006] utilize the ZK + semblance approach outlined in section 2.2. Comparisons between crustal estimates of R for particular seismic stations are made for those values with corresponding standard errors of less than ±0.06. This error threshold is chosen empirically as that which best partitions those receiver function stacks with visually recognizable energy along phase moveout curves from those where lack of data or poor quality make these moveout curves difficult to distinguish. For each study under comparison, data are reprocessed using the V_P chosen by the study authors. For the 2006 and 2007 studies the ZK + semblance method is used whereas for the Thompson et. al study the linear stacking ZK approach is employed. Both correlation coefficient and mean difference are provided in (Table 1) as measures of similarity.

		Correlation		Mean Difference	
Study Authors	Num. of Stns	H	R	H(km)	R
Thompson et. al. (2010)	29	0.97	0.70	0.49	0.012
Darbyshire et. al. (2007)	10	0.95	0.43	1.21	0.033
Eaton et. al. (2006)	26	0.90	0.61	0.79	0.025

Table 1: Comparison of R and H estimates with three published studies

All three studies reported H estimates that correlate strongly with the crustal thickness parameters computed here. The data from the northern Canadian Shield shows strong correlation in both H and R. The lower correlation observed in estimates of R than H is not unexpected as the range of R is relatively narrow and small changes ($\approx 2\%$) are physically meaningful. A corollary of this is greater sensitivity of R to differences in procedure such as the choice of deconvolution algorithm and selection and scaling of data. The results from Thompson et. al. [2010] also corrispond most closely to the parameter estimates computed here, with the mean difference for both parameters being less than half of the averaged bootstrap error computed in this study. Results published by *Eaton et. al.* [2006] show reasonable correlations in both R and H and a mean difference for both parameters that is roughly equal to the averaged uncertainty in the data. Parameter estimates from the Superior Province [Darbyshire et. al., 2007] show the lowest correlation in R as well as the highest mean difference in both parameters. These differences are well over the averaged computed error, and can not be easily explained by deviation related to noise in the data.

3.2 Full Grid Search Analysis

We now proceed to compare our results computed using the ZK approach with those from the full grid search (Table 2). We note that the velocity ratio R has a correlation between the two datasets of 0.76 whereas H has a correlation of 0.51. The low correlation between crustal thickness estimates can be explained by the strong tradeoff between H and V_P through the quantity

$$\frac{t_{Pps} - t_{Ps}}{2} = \frac{t_{Pss}}{2} - t_{Ps} = \frac{H}{V_P}\sqrt{1 - p^2V_P^2}.$$

As a consequence, contours of the misfit surface $s(H, R, V_P)$ are highly ex-

tended along the kinematic curve in the H - V_P space (Figure 5). This trade-off contributes to the low correlation in H between the two methods. Higher correlation in this quantity can be restored by dividing out V_P from H. The trade-off between the other parameters is lower as there is greater dependence between them such that a small change in one necessitates a large change in an other to maintain travel-time equality, which has the result of a well defined misfit surface (Figures 3-4.

For all but the cleanest stations, the trade-off between H and V_P renders recovery of V_P unfeasible using the full grid approach. A comparison between two stations, ULM, the station with the highest quality RFs, and DORN, a station exhibiting less resolution in the reflected phases, illustrates this difficulty. RFs are arranged vertically, ordered by increasing slowness, and shown in figures 2 and 6. Cross sections of $s(H, R, V_P)$ through each coordinate plane are displayed for ULM and DORN in figures 3-5) and figures 7-9. The lower resolution apparent in the H - V_P cross section for DORN translates into a bootstrap error of $V_P \pm 0.64$km/s. Station ULM, with cleaner data, has less trade-off between H and V_P as indicated by the corresponding cross section and the lower bootstrap error of $V_P \pm 0.16$km/s.

Active source experiments located near broadband seismic stations provide independent crustal thickness and P wave velocity estimates to test against data derived from the full parameter search method. We select stations with low error in V_P and active source experiment locations within a 100 km radius. If several active source experiments are located within this radius, estimates are averaged. Four stations (ARVN, TYNO, ULM and WHY) meet these criteria and the parameter estimates are presented in figure 10-11. Estimates computed from the full grid approach are roughly 0.25 km/s higher than the active source data. This difference is consistent across all four stations and is exemplified by a 99% correlation, suggesting possible bias. However, the limited number of data means this bias is poorly constrained.

There is less correlation between the crustal thickness data, though this is largely attributed to an approximate 10 km difference between the ARVN estimates. The reason for this discrepancy is unknown though both the ZK method and and a published study [Thompson et. al., 2010] provide an estimate of near 41 km for ARVN, much nearer the full grid value of 42 km. Despite lower correlation the apparent bias towards higher values computed from teleseismic data is also maintained for H. A positive bias in one parameter will tend to bias the other, owing to the relationship between

8

Parameter	correlation coeff
R (km)	0.76
H	0.51
H/V_P	0.96

Table 2: Correlation between parameters computed from ZK + semblance and full parameter search methods

thickness, velocity and times of a scattered phase. For a constant t_{ps} one may compute how much H must change for a 0.25 km/s bias in V_P [Zhu and Kanamori, 2000]. Using an average of the parameter estimates from the two cleanest stations, ULM and WHY, δH will be 1.3 km, this fits well with the actual bias in the values.

[[SOURCES REGARDING BIAS]] [[WHAT DOES THIS MEAN, IS VP USABLE FOR THE HIGHEST QUALITY STATIONS?]]

3.3   Crustal Discontinuities

We now consider the average crustal structure across Canada. We produce a depth profile for each station by stacking receiver functions along traveltime curves corresponding to a range of values in H (0 to 50 km in increments of 100 metres) using the estimates for R computed via the ZK + semblance method. The resulting profiles contain energy at depths corresponding to major velocity discontinuities. By assembling all depth profiles into a matrix, we may decompose the data via SVD into their principal components. Figure 12 contains the first five singular vectors or modes normalized to unit magnitude that account for 78% of the variance in the profiles. Higher modes correspond to diminishing contributions to total variance. Each vector is normalized to unit magnitude. The first mode (blue) is effectively the average depth profile across all stations and captures 50% of the variance in the dataset. It features a maximum near 38.7 km that may be taken as an average Moho depth. The second and third modes are dominated by a high amplitude shallow structures (e.g. sedimentary layers) within the top 10 km and Moho variability between 30 and 46 km . The fourth and fifth modes account for a combined 11% of the variance in the dataset, contain energy at upper-mid crustal depths in the 10 km to 20 km range. All 5 modes display markedly lower energy within a depth window roughly between 20 km and 30 km.
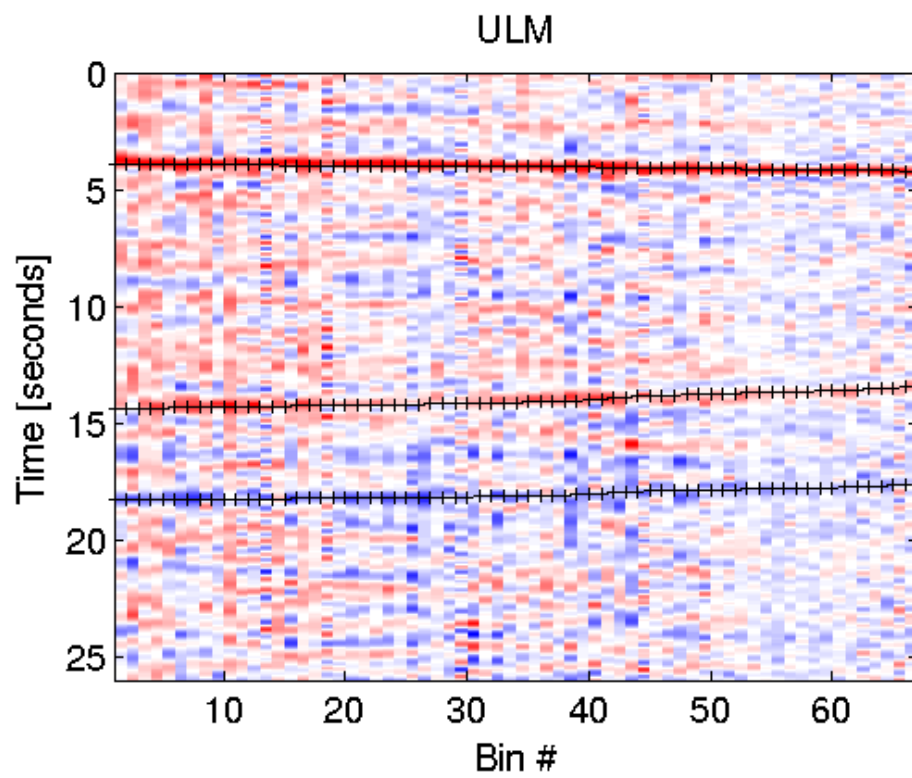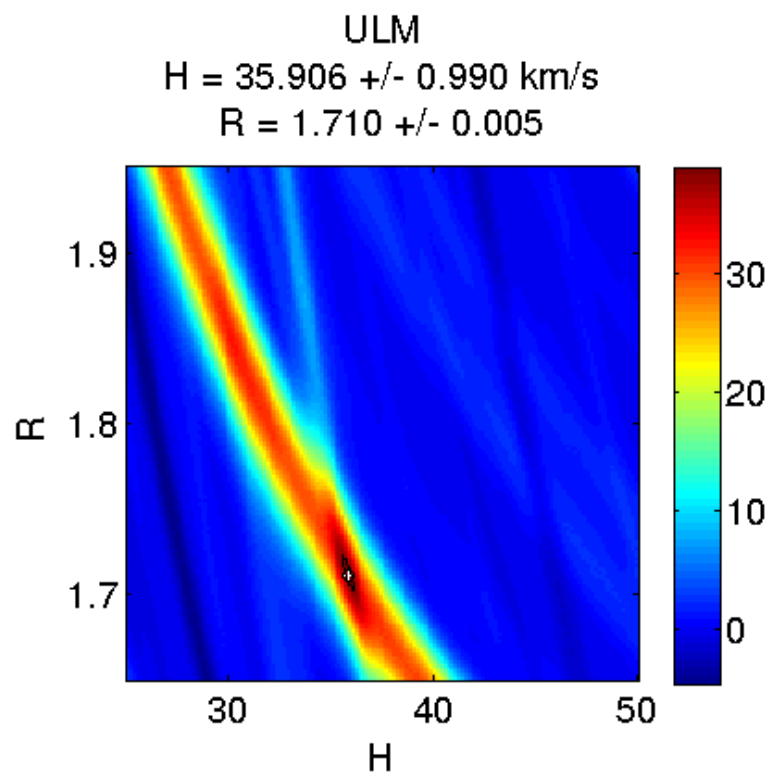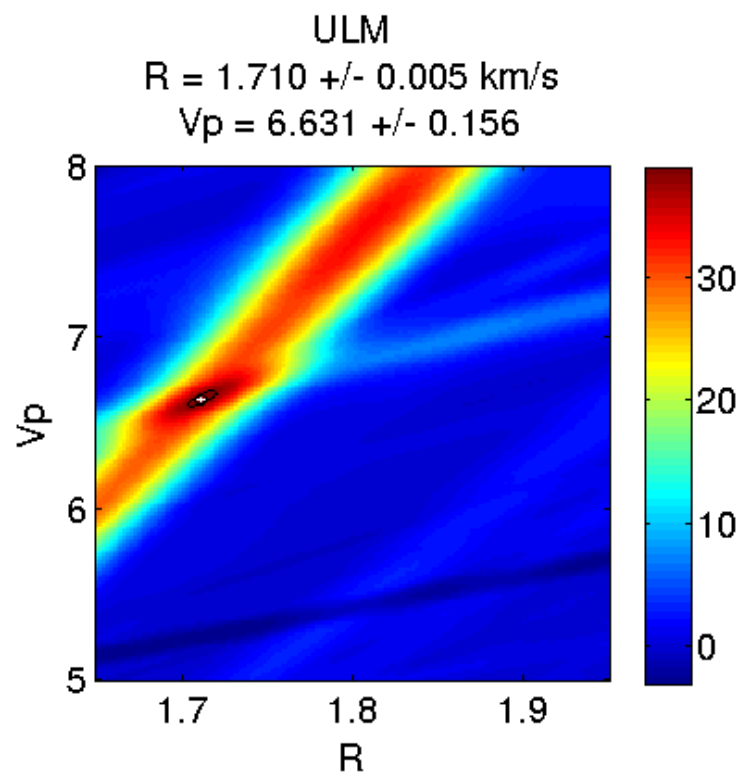
Figure 2:

Figure 3:

ULM
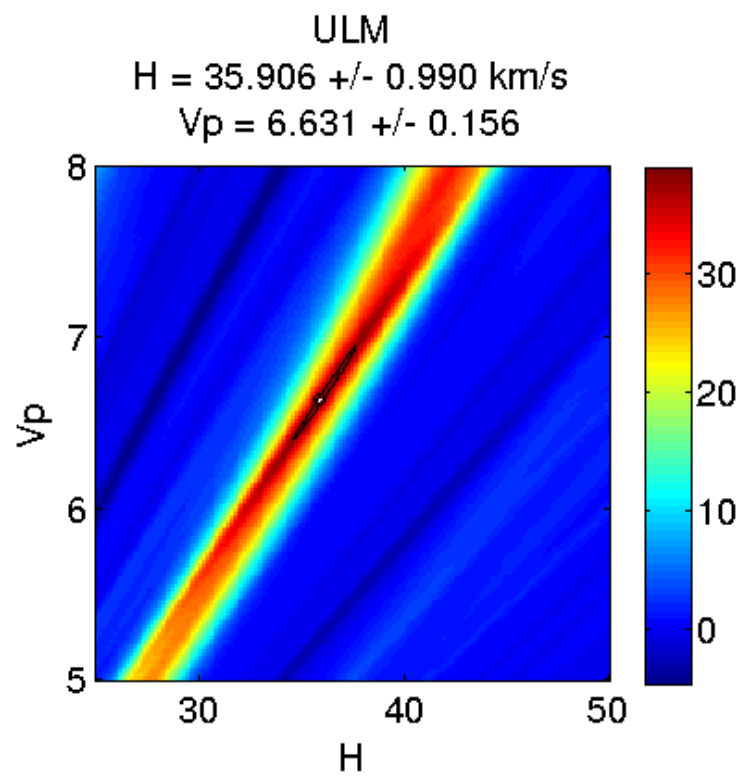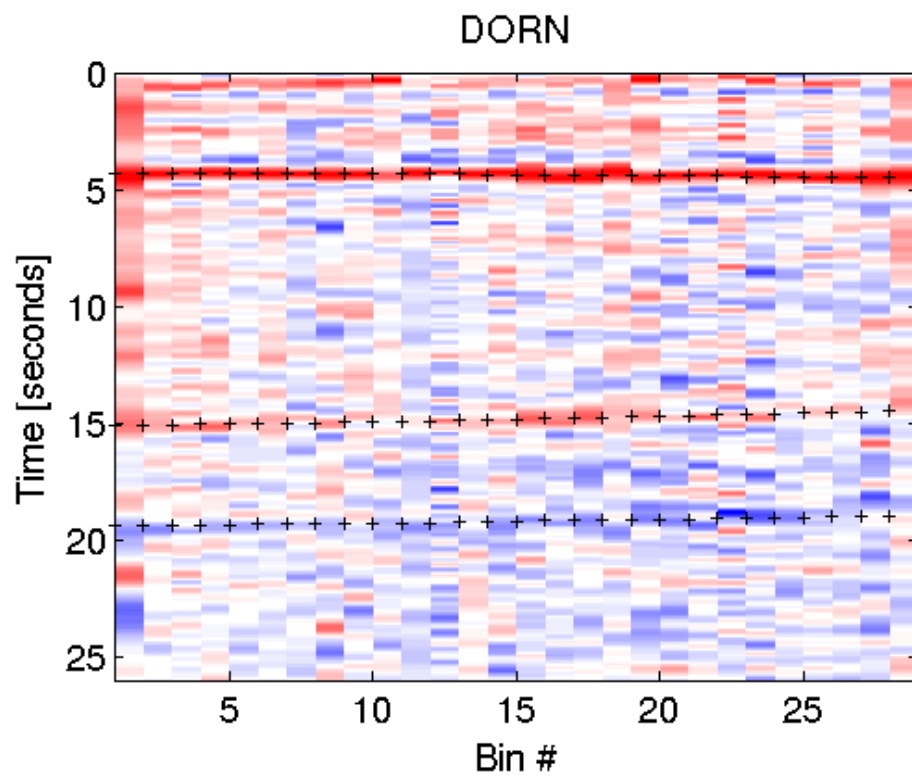R = 1.710 +/- 0.005 km/s
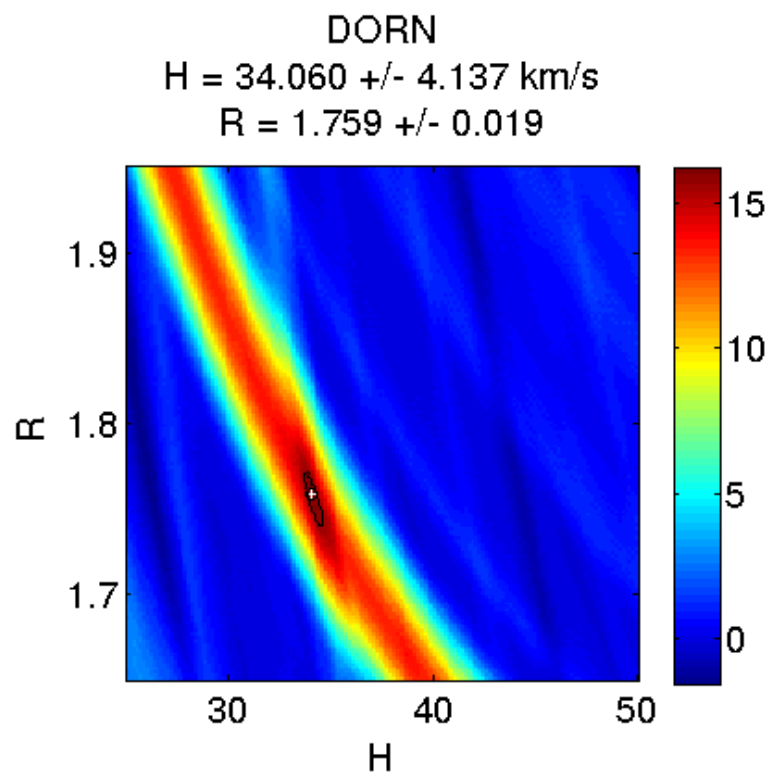Vp = 6.631 +/- 0.156
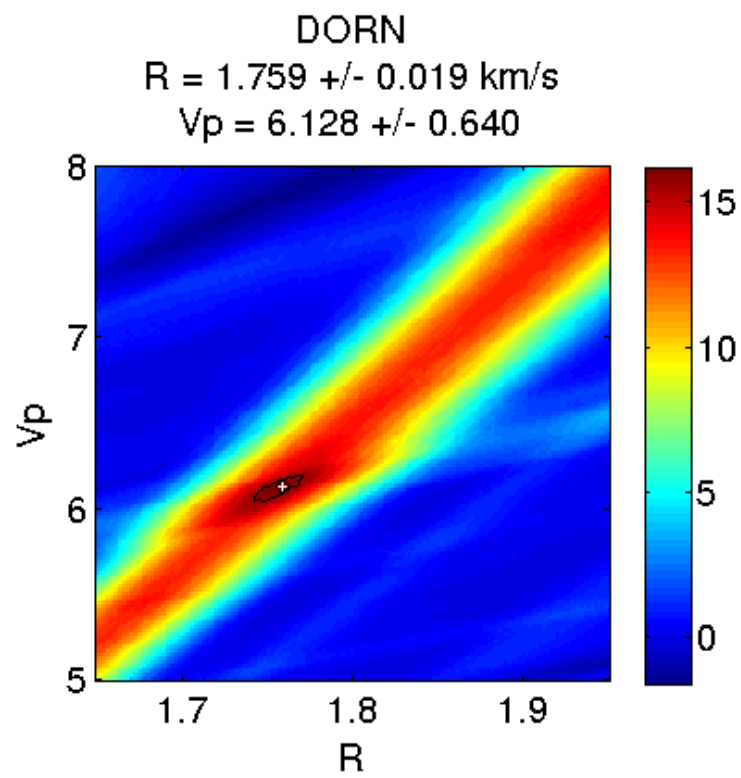
Figure 4:

12

Figure 5:

Figure 6:

14

Figure 7:

Figure 8:

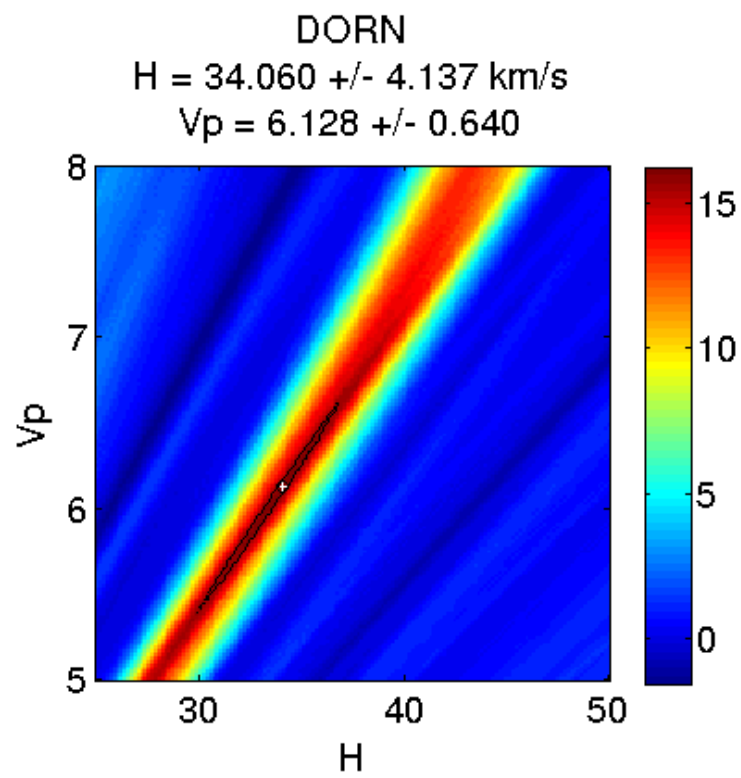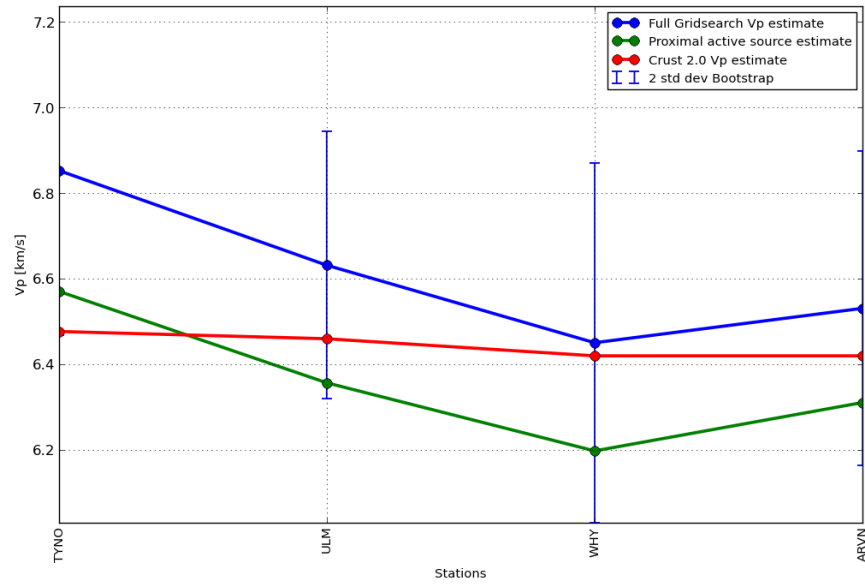Figure 9:

Figure 10: *P wave velocity estimates computed from the full parameter search method compared to active source data and values from Crust 2.0*
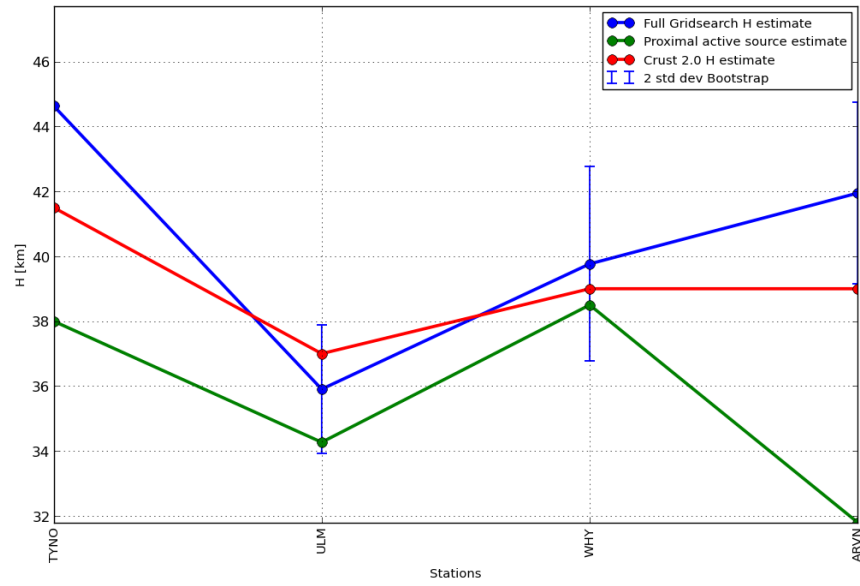
Figure 11: Crustal thickness estimates computed from the full parameter search method compared to active source data and values from Crust 2.0
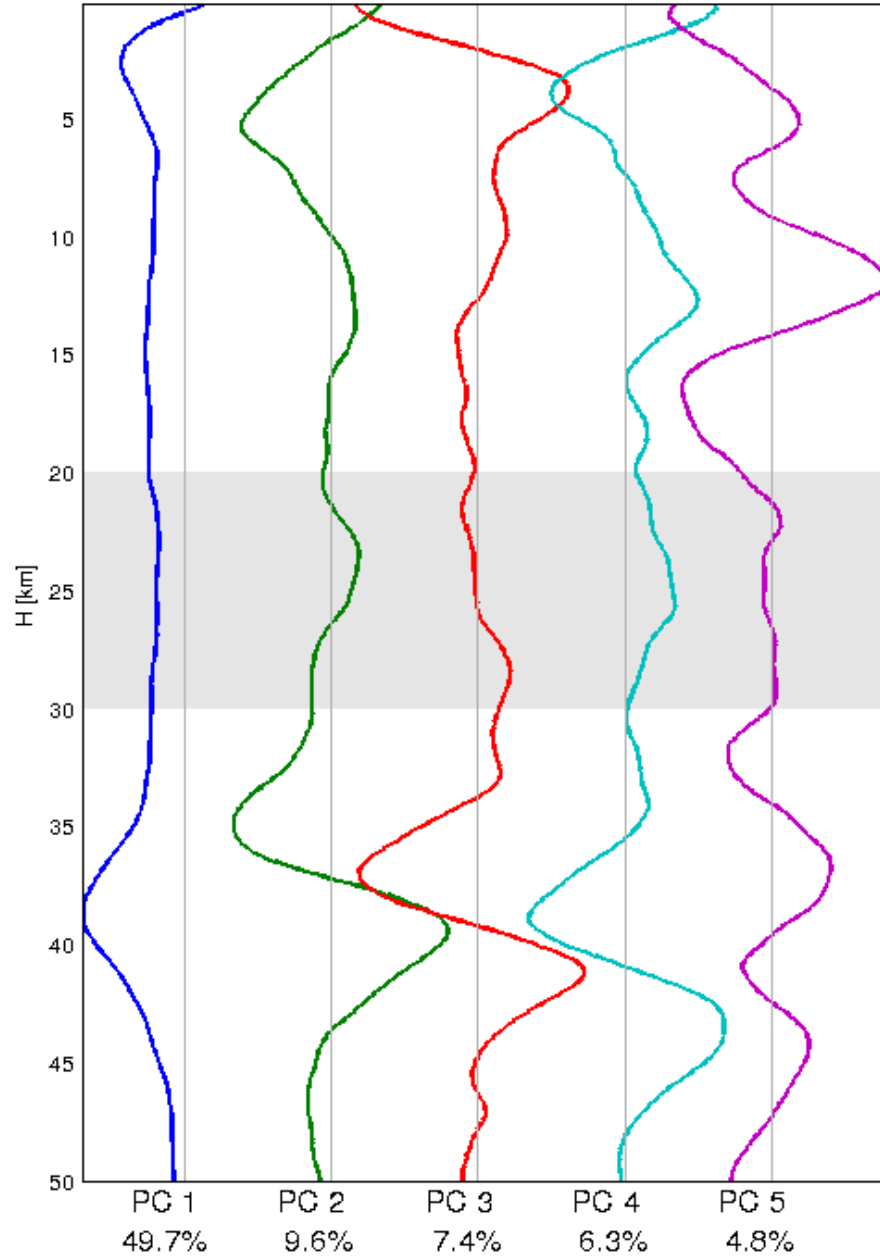
Figure 12: The SVD singular vectors (principal components) of the station depth profile matrix. Each principal component represents a mode that captures some part of the total variance in the dataset. Vertical lines are the axis each profile and vector is normalized about. A grey horizontal window highlights a region of low energy.

3.4 Regional Bulk Crustal Parameters

We proceed to consider crustal thickness H and velocity ratio, R, estimates for stations with assigned R bootstrap errors below ± 0.06 in a geographic context (figure 13). To compensate for the uneven distribution of seismic stations, weights are applied to both R and H estimates before averaging over a given region. Weights are calculated by projecting station locations onto a 2D plane using the Albers equal-area conic projection. A Voronoi diagram is then computed using all projected station locations. The ratio between the Voronoi cell surface encompassing each station and the total area of the convex hull bounding region is employed as that station's weight.

Table 3 displays the results of our regionalization in R and H. The weighted average crustal thickness for all stations (Canada) is 37 km, about two kilometres thinner than the average for the Canadian Shield. Crust 2.0 provides a slightly thicker crustal average for Canada (38.2 km) and a slightly thinner average for the Shield (38.8 km). The Slave Province averages are similar to those for the Churchill province and a thicker crust than Crust2.0 and a smaller seismic velocity ratio. Moving south and east from the Churchill Province through the Superior Province into the Grenville Province, we note an increase in the ZK + semblance R values as well as crustal thickness H, figures 14-15. The weighted R average is 1.73 in the Churchill Province increasing slightly to 1.74 in the Superior and jumping to 1.78 in the Grenville. In a similar fashion, the weighted average of H increases from 38.9 km in the Churchill Province to 39.7 in the Superior Province and 41.7 km in the Grenville Province. The southeastern trend towards increasing values is also expressed in weighted averaged active source V_P data. The Crust 2.0 model is characterized by slightly thinner crust though the southward thickening trend is noticeable. The trend in the seismic velocity is not, however, as apparent.

4 Discussion

4.1 Canada

- Quiet zone in discontinuity data
- Compare data to Crust 2.0. What do the differences mean.
    - Lith 5.0 data?

	ZK + semblance		Crust 2.0		Active Source
Region	$H[km]$	R	$H[km]$	R	$V_P[km/s]$
Canada	37.0	1.75	38.2	1.77	6.33
Shield	39.2	1.74	38.8	1.77	6.42
Slave	38.2	1.74	37.0	1.76	6.44
Churchill	38.9	1.73	37.8	1.77	6.39
Superior	39.7	1.74	39.1	1.76	6.44
Grenville	41.7	1.78	40.5	1.78	6.48

Table 3: Comparison of R and H estimates with three published studies
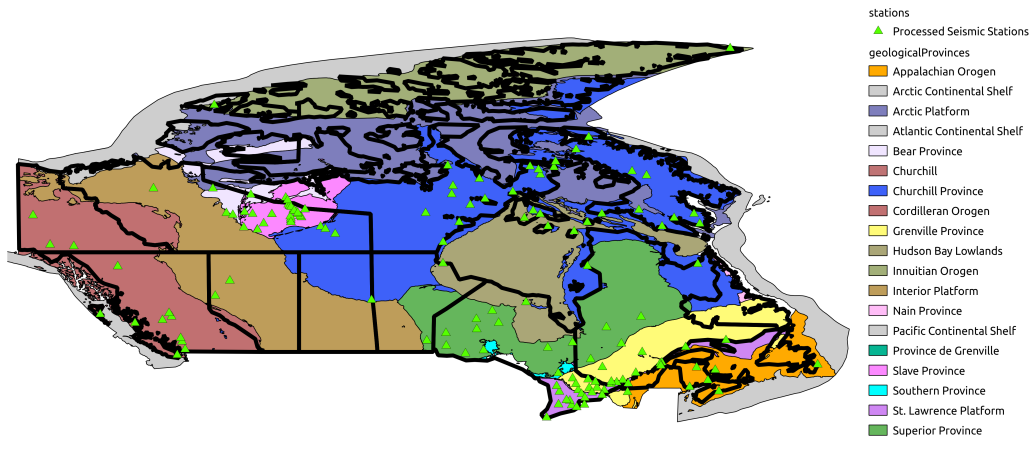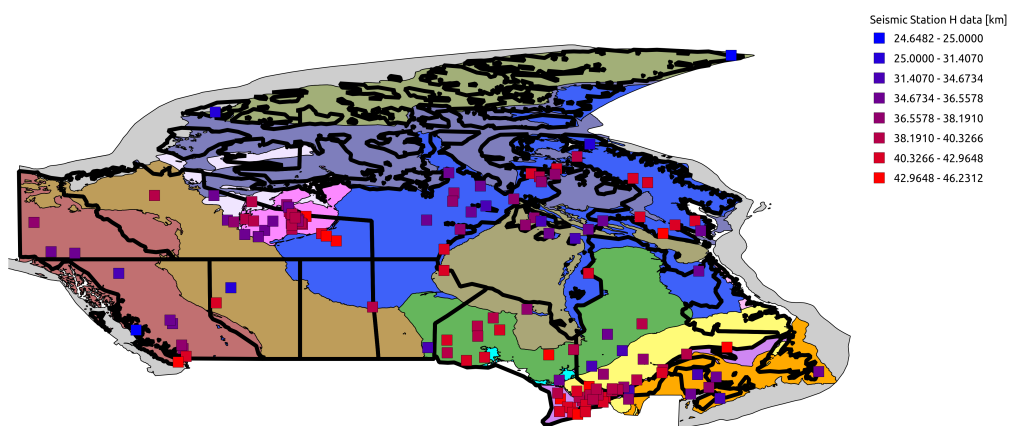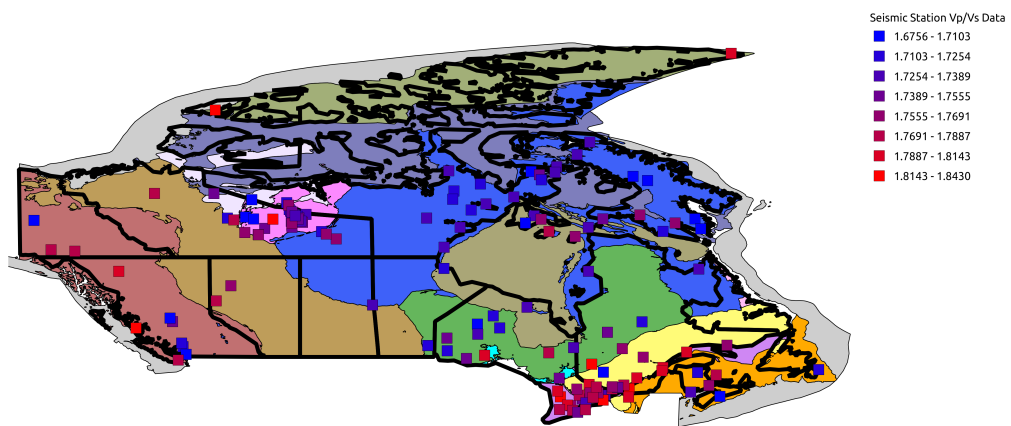

Figure 13:

22

Figure 14:

Figure 15:

- Discuss spatial trends -¿ high R -¿ Low R moving North West through Ontario

    - this is part of larger trend of changing R values as we move from Churchill to Grenville

    - in the literature? Yes. See notes on lithoprobe studies

- Secular variation in NE Churchill from thinner crusts to thicker as we move East

    - in the literature? See Lith 5.0: A revised crustal model for Canada based on lithoprobe results.

- Explanation of results

- Canada H and Vp/Vs

- Lith5.0 (Perry, 2002) estimates for Canadian crustal averages is 38 km. The Crust 2.0 average is 38 km as well, however this is expected since Crust2.0 data for Canada is based on the same data as that of Lith5.0 .... is it definately?

- Make some comparison to global average?

5 Conclusions

6 bibliography

Bassin, C., G. Laske, G. Masters (2000), The Current Limits of Resolution for Surface Wave Tomography in North America, EOS Trans AGU, 81.

Bostock, M. G. (1998), Mantle stratigraphy and the evolution of the Slave province, J. Geophys. Res., 103, 21183-21200.

Bostock, M. G., M. R. Kumar (2010), Bias in seismic estimates of crustal properties, J. Geophys. Int., 182, 403-407.

Christensen, N. I. (1996), Poisson's ratio and crustal seismology, J. Geophys. Res., 101, 31393156.

Darbyshire, F. A., D. W. Eaton, A. W. Frederiksen, E. Leila (2006), New insights into the lithosphere beneath the Superior Province from Rayleigh

wave dispersion and receiver function analysis, J. Geophys. Int., 169, 1043-1068.

Durrheim, R. J., W. D. Mooney (1991), Archean and Proterozoic crustal evolution, Geology, 19, 606-609.

Eaton, D. W., S. Dineva, R. Mereu (2005), Crustal thickness and Vp/Vs variations in the Grenville orogen (Ontario, Canada) from analysis of teleseismic receiver functions, Tectonophysics, 420, 223-238.

Efron, B., R. Tibshirani (1986), Bootstrap Methods for Standard Errors, Confidence Intervals, and Other Measures of Statistical Accuracy, Statistical Science, 1, 54-75.

Golub, G. H., M. Heath, G. Wahba (1979), Generalized cross-validation as a method for choosing a good ridge parameter, Technometrics, 21, 215-223. Mooney, W. D. (2012), Personal communication. Compiled GSC active source data for the Canada.

Kennet, B. L. N., (1991), The removal of free surface interactions from three-component seismograms, J. Geophys. Int., 104, 153-163.

Langston, C. A. (1979), Structure under Mount Rainier, Washington, inferred from teleseismic body waves, J. Geophys. Res., 84(B9), 47494762, doi:10.1029/JB084iB09p04749.

Perry, H. K. C., D. W. S. Eaton, A. M. Forte (2002) LITH5.0: a revised crustal model for Canada based on Lithoprobe results, J. Geophys. Int., 150, 285-294.

Thompson, D. A., I. D. Bastow, G. Helffrich, J.-M. Kendall, J. Wookey, D. B. Snyder, D. W. Eaton (2010), Precambrian crustal evolution: Seismic constraints from the Canadian Shield, Earth and Planetary Science Letters, 297, 655666.

Zhu, L., H. Kanamori (2000), Moho depth variation in Southern California from teleseismic receiver functions, J. Geophys. Res., 105, 2969-2980.

Zandt, G., C. J. Ammon (1995), Continental crust composition constrained by measurements of crustal Poisson's ratio, Nature, 374, 152-154.